

The Impact of Moist Physics on the Sensitive Area Identification for Heavy Rainfall Associated Weather Systems

Huizhen YU, Zhiyong MENG

Citation: Yu, H. Z., Z. Y. Meng, 2022: The Impact of Moist Physics on the Sensitive Area Identification for Heavy Rainfall Associated Weather Systems, *Adv. Atmos. Sci.*, In press. doi: [10.1007/s00376-021-0278-9](https://doi.org/10.1007/s00376-021-0278-9).

View online: <https://doi.org/10.1007/s00376-021-0278-9>

Related articles that may interest you

[Analysis of Spatial Autocorrelation Patterns of Heavy and Super-Heavy Rainfall in Iran](#)

Advances in Atmospheric Sciences. 2017, 34(9), 1069 <https://doi.org/10.1007/s00376-017-6227-y>

[The Initial Errors in the Tropical Indian Ocean that Can Induce a Significant “Spring Predictability Barrier” for La Nia Events and Their Implication for Targeted Observations](#)

Advances in Atmospheric Sciences. 2021, 38(9), 1566 <https://doi.org/10.1007/s00376-021-0427-1>

[A Numerical Study of Mesoscale Vortex Formation in the Midlatitudes: The Role of Moist Processes](#)

Advances in Atmospheric Sciences. 2019, 36(1), 65 <https://doi.org/10.1007/s00376-018-7234-3>

[A Three-dimensional Wave Activity Flux of Inertia-Gravity Waves and Its Application to a Rainstorm Event](#)

Advances in Atmospheric Sciences. 2019, 36(2), 206 <https://doi.org/10.1007/s00376-018-8018-5>

[Model Uncertainty Representation for a Convection-Allowing Ensemble Prediction System Based on CNOP-P](#)

Advances in Atmospheric Sciences. 2020, 37(8), 817 <https://doi.org/10.1007/s00376-020-9262-z>

[An Adjoint-Free CNOP-4DVar Hybrid Method for Identifying Sensitive Areas in Targeted Observations: Method Formulation and Preliminary Evaluation](#)

Advances in Atmospheric Sciences. 2019(7), 721 <https://doi.org/10.1007/s00376-019-9001-5>



AAS Website



AAS Weibo



AAS WeChat

Follow AAS public account for more information

• Original Paper •

The Impact of Moist Physics on the Sensitive Area Identification for Heavy Rainfall Associated Weather Systems[✉]

Huizhen YU¹ and Zhiyong MENG^{*2}¹*Qingdao Meteorological Bureau, Qingdao 266003, China*²*Department of Atmospheric and Oceanic Sciences, School of Physics, Peking University, Beijing 100871, China*

(Received 28 August 2020; revised 27 May 2021; accepted 28 June 2021)

ABSTRACT

The impact of moist physics on the sensitive areas identified by conditional nonlinear optimal perturbation (CNOP) is examined based on four typical heavy rainfall cases in northern China through performing numerical experiments with and without moist physics. Results show that the CNOP with moist physics identifies sensitive areas corresponding to both the lower- (850–700 hPa) and upper-level (300–100 hPa) weather systems, while the CNOP without moist physics fails to capture the sensitive areas at lower levels. The reasons for the CNOP peaking at different levels can be explained in both algorithm and physics aspects. Firstly, the gradient of the cost function with respect to initial perturbations peaks at the upper level without moist physics which results in the upper-level peak of the CNOP, while it peaks at both the upper and lower levels with moist physics which results in both the upper- and lower-level peaks of the CNOP. Secondly, the upper-level sensitive area is associated with high baroclinicity, and these dynamic features can be captured by both CNOPs with and without moist physics. The lower-level sensitive area is associated with moist processes, and this thermodynamic feature can be captured only by the CNOP with moist physics. This result demonstrates the important contribution of the initial error of lower-level systems that are related to water vapor transportation to the forecast error of heavy rainfall associated weather systems, which could be an important reference for heavy rainfall observation targeting.

Key words: moist physics, heavy rainfall, sensitive area, CNOP

Citation: Yu, H. Z., and Z. Y. Meng, 2022: The impact of moist physics on the sensitive area identification for heavy rainfall associated weather systems. *Adv. Atmos. Sci.*, **39**(5), 684–696, <https://doi.org/10.1007/s00376-021-0278-9>.

Article Highlights:

- With moist physics, CNOP identifies both the upper-level and lower-level sensitive areas. Without moist physics, CNOP only identifies the upper-level sensitive area.
- The gradient of the cost function with respect to initial perturbations peaks at the upper levels without moist physics, while it peaks at both upper and lower levels with moist physics.
- The upper-level sensitive area is associated with high baroclinicity, and the lower-level sensitive area is associated with moist processes.

1. Introduction

Heavy rainfall is one of the main severe weather events that can lead to disaster in China by threatening lives and causing great economic losses (Zhang, 2006; Chen and Gao, 2010). Many field experiments and studies have been implemented to investigate the dynamic mechanisms that lead to heavy rainfall events and their predictability (Ni et

al., 2006; Wang et al., 2014a). Heavy rainfall is usually caused by the nonlinear interaction of multiscale weather systems (Liu et al., 2011; Li et al., 2014; Qi and Xu, 2018). Small errors in the initial conditions may result in large differences in the forecasts (Lorenz, 1963; Zhu et al., 2007). In order to improve heavy rainfall forecasts, it is important to find the key factors contributing to their large error growth.

Sensitivity analysis can reveal how numerical forecast or simulation results respond to changes in initial conditions. Sensitivity analysis has been used to study the practical and intrinsic predictability of mesoscale weather systems (Zhang et al., 2003, 2006). Sippel and Zhang (2010) used sensitivity analysis to reveal the factors affecting the predictability of Hurricane Humberto and the origins of trop-

✉ This paper is a contribution to the special issue on Predictability, Data Assimilation and Dynamics of High Impact Weather—In Memory of Dr. Fuqing ZHANG.

* Corresponding author: Zhiyong MENG
Email: zymeng@pku.edu.cn

ical cyclone intensity forecast error. Sensitivity analysis based on global operational ensemble forecasts has also been used to identify key processes contributing to extremely heavy rainfall events (Schumacher, 2011; Lynch and Schumacher, 2014; Yu and Meng, 2016; Zhang and Meng, 2018).

Two major groups of methods have been applied to sensitivity analysis. One is ensemble-based methods, such as ensemble Kalman filter (EnKF; Hamill and Snyder, 2002), ensemble transform Kalman filter (ETKF; Bishop et al., 2001), and ensemble-based sensitivity analysis (ESA; Hakim and Torn, 2008). The other is based on adjoint technology, such as singular vectors (SVs; Palmer et al., 1998) and adjoint sensitivity analysis (Mahfouf and Bilodeau, 2007; Doyle et al., 2019; Reynolds et al., 2019). A major limitation in most current methods is the linear assumption for error growth, which may lead to incorrect results (Reynolds and Rosmond, 2003; Huang and Meng, 2014). Taking nonlinear processes into account, conditional nonlinear optimal perturbation (CNOP) method was proposed by Mu and Duan (2003) to examine the predictability and target area of atmospheric and oceanic processes. CNOP-I (hereafter called CNOP) is the initial perturbations whose nonlinear evolution attains the maximum of a given cost function under certain constraints. The CNOP method has been applied to predictability and sensitivity analysis for many high-impact events such as tropical cyclones, Kuroshio large meander (KLM), and El Niño-Southern Oscillation (ENSO) (Wang and Mu, 2017). The CNOP method has also been applied in the study of heavy rainfall, which shows that a decrease in CNOP-type initial error could improve forecasts (Mu et al., 2007). Yu and Meng (2016) used the CNOP based on MM5 to find the key weather systems that influenced the simulation of the heavy rainfall in Beijing on 21 July 2012. Their results showed that the key weather system found by CNOP is a low-level vortex, which is consistent with the diagnostic results obtained by Meng et al. (2013). These results suggest that the CNOP method may be a good way to find the key weather systems leading to heavy rainfall (Yu and Meng, 2016).

Moist physics is quite important for heavy rainfall (Wang et al., 2014b; Joseph et al., 2015; Li et al., 2016) and adjoint-based sensitivity analysis (Ehrendorfer and Errico, 1995; Jung and Kim, 2009). Many studies have shown that rapid error growth is closely associated with moist physics (Ehrendorfer et al., 1999; Zhang et al., 2002, 2003) for heavy rainfall events (Zhang et al., 2006; Liu and Tan, 2009; Zhu et al., 2009; Zhang et al., 2016b). These studies suggest that it is important to understand how moist physics may influence the identification of sensitive areas for heavy rainfall cases. Previous results have shown that SVs calculated with moist physics differ from and grow faster than SVs calculated without moist physics (Ehrendorfer et al., 1999; Coutinho et al., 2004). However, the influences of moist physics on CNOP remain unknown.

Most previous atmospheric research studies using the

CNOP method were based on MM5 (Grell et al., 1995) and its tangent linear and adjoint models (Zou et al., 1997). With the WRF model gradually replacing the MM5, a WRF-based tool to calculate CNOP was established (Yu et al., 2017). The results were compared with the MM5 based on the dry model configuration since the moist physics (i.e., large-scale precipitation and convection) in the WRF adjoint model have not been fully developed (Yu et al., 2017). Understanding the limitations of using a dry model configuration for CNOP, especially for heavy rainfall cases, is important and will be addressed in this study by performing experiments with and without moist physics.

This study is aimed at examining the impact of moist physics on CNOP and the associated sensitive area identification based on four heavy rainfall cases using MM5. The CNOP method is described in section 2. The heavy rainfall cases and experiment design are introduced in section 3. The results are discussed in section 4. Finally, a summary is provided in section 5.

2. A brief introduction to the CNOP method

CNOP refers to the initial perturbations that maximize the cost function J at a specified time under chosen constraint conditions (Mu and Duan, 2003). J is defined as the average of the total dry energy perturbations (TDE') in the verification area at the verification time. Suppose we have a nonlinear model as follows:

$$\begin{cases} \frac{\partial \mathbf{x}}{\partial t} + \mathbf{F}(\mathbf{x}) = 0 \\ \mathbf{x}|_{t=0} = \mathbf{x}_0 \end{cases}, \quad (1)$$

where \mathbf{x} and \mathbf{F} are the state vector and the nonlinear partial differential operator of the model. \mathbf{x}_0 is a value of \mathbf{x} at the initial time and $\mathbf{x}(t)$ is the value of \mathbf{x} at forecast time t . $\mathbf{x}(t) = \mathbf{M}(\mathbf{x}_0)$, where \mathbf{M} is the nonlinear operator (nonlinear MM5 model in this study). CNOP is defined as the initial perturbations $\delta \mathbf{x}_0^*$ that satisfy the following equation:

$$J(\delta \mathbf{x}_0^*) = \max_{\delta \mathbf{x}_0^T \mathbf{C}_1 \delta \mathbf{x}_0 \leq \beta} (J(\delta \mathbf{x}_0)), \quad (2)$$

where

$$J = \frac{1}{D} \int_D \int_0^1 \frac{1}{2} (u'^2 + v'^2 + \frac{C_p}{T_r} T'^2) d\eta dD + \frac{1}{D} \int_D \frac{1}{2} R_a T_r \left(\frac{P'_s}{P_r} \right)^2 dD. \quad (3)$$

The initial perturbations are constrained by the total dry energy via $\delta \mathbf{x}_0^T \mathbf{C}_1 \delta \mathbf{x}_0 \leq \beta$. D and η represent the horizontal verification area and the vertical level, respectively. The verification area is the area of interest where the minimized forecast error is expected. C_p ($1005.7 \text{ J kg}^{-1} \text{ K}^{-1}$) is the specific heat at constant pressure. T_r (270 K) is the reference temperature. R_a ($287.04 \text{ J kg}^{-1} \text{ K}^{-1}$) is the gas constant of dry air. P_r

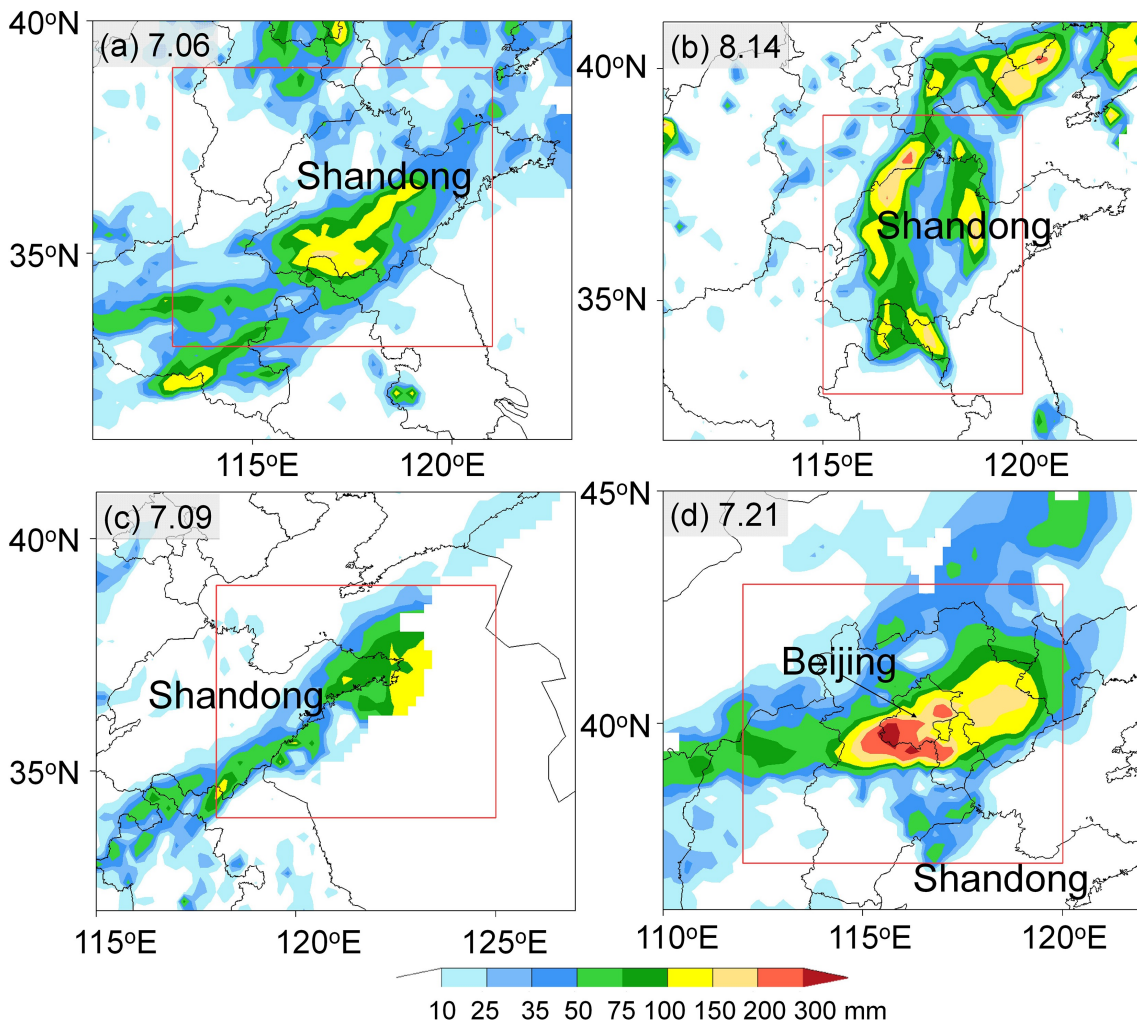


Fig. 1. The distribution of 24-h accumulated precipitation (shaded; units: mm), (a) from 0000 UTC 6 July to 0000 UTC 7 July 2017 for the “7.06” case; (b) from 1200 UTC 13 August to 1200 UTC 14 August 2018 for the “8.14” case; (c) from 0000 UTC 9 July to 0000 UTC 10 July 2018 for the “7.09” case; (d) from 0000 UTC 21 July to 0000 UTC 22 July 2012 for the “7.21” case. The inner red box denotes the verification area in the corresponding case.

(1000 hPa) is the reference pressure. u' , v' , T' , and P'_s are the forecast differences of zonal and meridional wind components, temperature, and surface pressure, respectively. The base states of the above variables are the model simulations without initial perturbations.

The total dry energy (TDE) metric was used to ensure consistency between the experiments with and without moist physics. TDE is associated with the perturbations of u , v , T , and P_s , which represent the dynamic and thermodynamic features of the weather systems that are associated with heavy rainfall events. Changes in these fundamental variables will eventually change the evolution of moisture and thus precipitation. TDE has been used for many predictability studies since it is suggested as a first-order approximation of the analysis error covariance metric (Molteni et al., 1996; Palmer et al., 1998). Even though the total moist energy (TME) could be a more suitable metric for heavy rainfall cases in practice, this study is aimed at examining the

impact of moist physics on the sensitive area identifications for the weather systems that are associated with heavy rainfalls. What we are interested in is how the moist physics may affect the identification of sensitive areas in terms of the dynamic and thermodynamic features of the background weather systems without perturbing the moisture variables, thus the metric and perturbed variables are the same between the experiments with and without moist physics. Using TME as the constraint metric would make the comparison not apple-to-apple because there are no moisture perturbation variables in the dry run.

Vertically integrated total energy has been widely used to define the sensitive area identified by the SV (Buizza and Montani, 1999; Buizza et al., 2007), in field campaigns such as FASTEX (Montani et al., 1999) and T-PARC (Kim et al., 2011), and in data-assimilation experiments carried out with the ECMWF (Buizza et al., 2007; Cardinali et al., 2007). These observation experiments demonstrated the validation

of the SV-based sensitive area defined by the vertically integrated total energy. Vertically integrated total energy has also been used to define the sensitive area identified by the CNOP, and observation system experiment results have shown that assimilating extra data in this defined target area is effective in improving the forecast of a typhoon's track (Chen, 2011). Zhou and Zhang (2014) compared the horizontal projection, single energy projection, and vertically integrated energy schemes to define the sensitive area identified by the CNOP for typhoon observation targeting, and the results showed that the vertically integrated energy scheme was the best. These previous results suggest that the vertically integrated total energy should be valid to define the sensitive area identified by the CNOP for heavy rainfall. Validation of using vertically integrated total energy to identify sensitive areas has also been demonstrated for typhoon and winter storm events (Yu et al., 2017) and heavy rainfall events (Yu and Meng, 2016).

In this study, the sensitive area identified by the CNOP is defined as the location of the top 1% vertically integrated TDE' (vTDE') of all model grid points. In this area, the initial perturbations may have the largest impact on the forecast TDE'. The optimization algorithm of the spectral projected gradient 2 (SPG2; Birgin et al., 2001), which has been generally used to calculate the minimum value of a function of several variables subject to a constraint, was applied to calculate the CNOP (Yu et al., 2017).

3. Cases and experimental design

Four heavy rainfall cases, which represent four typical heavy rainfall processes that frequently occur in northern China, were examined in this study. They are the "7.06" case associated with a subtropical cyclone, the "8.14" case associated with a tropical cyclone, the "7.09" case associated with a shear line, and the "7.21" case associated with a lower-level vortex. In the "7.06" case, the 24-h precipitation of above 50 mm from 0000 UTC 6 July to 0000 UTC 7 July 2017 was mainly located in southwestern Shandong Province with a maximum value of 188.1 mm (Fig. 1a). In the "8.14" case, the 24-h precipitation of above 50 mm from 1200 UTC 13 August to 1200 UTC 14 August 2018 was mainly located in western Shandong (Fig. 1b). In the "7.09" case, the 24-h precipitation of above 50 mm from 0000 UTC 9 July to 0000 UTC 10 July 2018 was mainly located in eastern Shandong (Fig. 1c). In the "7.21" case, the 24-h precipitation from 0000 UTC 21 July to 0000 UTC 22 July 2012 averaged over the Beijing metropolitan area was about 190 mm (Fig. 1d), which broke the meteorological record of Beijing since 1951 (Xu et al., 2012). The rainfall observations are at 1-h intervals and are provided by the China Meteorological Administration (CMA).

In this study, considering that the adjoint of moist physical processes in WRF has not been fully developed, the MM5 and its tangent linear and adjoint versions were used to calculate the CNOP. In this study, the same model configura-

tion was set for the nonlinear, tangent linear, and adjoint models. The model domain for this study is a 91(lat) × 101(lon) horizontal grid with a horizontal resolution of 60 km and 21 evenly spaced sigma levels in the vertical from the surface to 50 hPa. The initial and boundary conditions are provided by the National Centers for Environmental Prediction final analysis (NCEP FNL) of 1°×1° at a 6-h interval. The nonlinear model simulations with the initial and boundary conditions were considered the base state. The verification area covers the location of heavy rainfall (inner red box in Fig. 1), and the simulation time covers the main stage of the heavy rainfall in the verification area. The starting and ending times of the 24-h accumulated rainfall mentioned above were set as the initial and verification times of the model integration. For each case, in order to find out the impact of moist physics on sensitive area identification, two experiments were performed with exactly the same configuration except for different moist physical processes: large-scale precipitation was considered with the Anthes-Kuo cumulus parameterization scheme used for the moist simulations (EXP_moist), whereas the dry simulations (EXP_dry) were run with the microphysical processes and cumulus parameterization scheme all turned off (Hoskins et al., 2000; Coutinho et al., 2004). The bulk planetary boundary layer scheme was used for both experiments. In EXP_moist, the patterns of the simulated heavy rainfall events (Fig. 2) are generally consistent with the observations (Fig. 1) except that the model results slightly underestimate the rainfall amount.

4. Result

4.1. Sensitive areas identified by the CNOP

For the "7.06" case, two sensitive areas (top 1% vTDE') are identified by the CNOP in EXP_moist (A, B in Fig. 3a). Sensitive area A is located to the southwest of the verification area, and the vertical distribution of the horizontally integrated TDE' (hereafter referred to as hTDE') over area A peaks at an upper level (~300 hPa, black line in Fig. 3b). Sensitive area B is located at the southwest corner of the verification area, and the hTDE' over it peaks at lower levels (~700 hPa, red line in Fig. 3b). However, in EXP_dry, only one sensitive area, peaking at upper levels similar to sensitive area A in EXP_moist, is identified by the CNOP (A in Figs. 3c and 3d).

The location of TDE' relative to the weather systems at the level of peak hTDE' is also presented (Fig. 4). Sensitive area A in EXP_moist is located over the base of a westerly trough at 300 hPa (Fig. 4a). Sensitive area B in EXP_moist is located in front of the trough associated with the subtropical cyclone at 700 hPa (Fig. 4b). The location and corresponding weather system of sensitive area A in EXP_dry are similar to sensitive area A in EXP_moist (Fig. 4c). This result shows that both the CNOPs in EXP_moist and EXP_dry capture sensitive areas corresponding to the westerly trough at upper levels, while the CNOP in EXP_moist also cap-

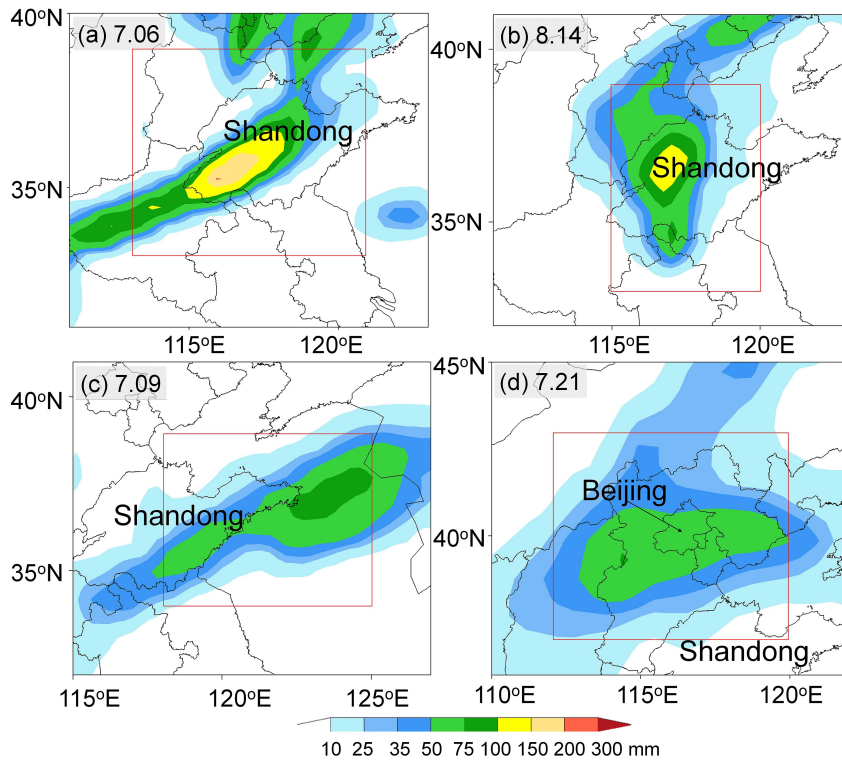


Fig. 2. Same as Fig. 1 but for the MM5 simulation results.

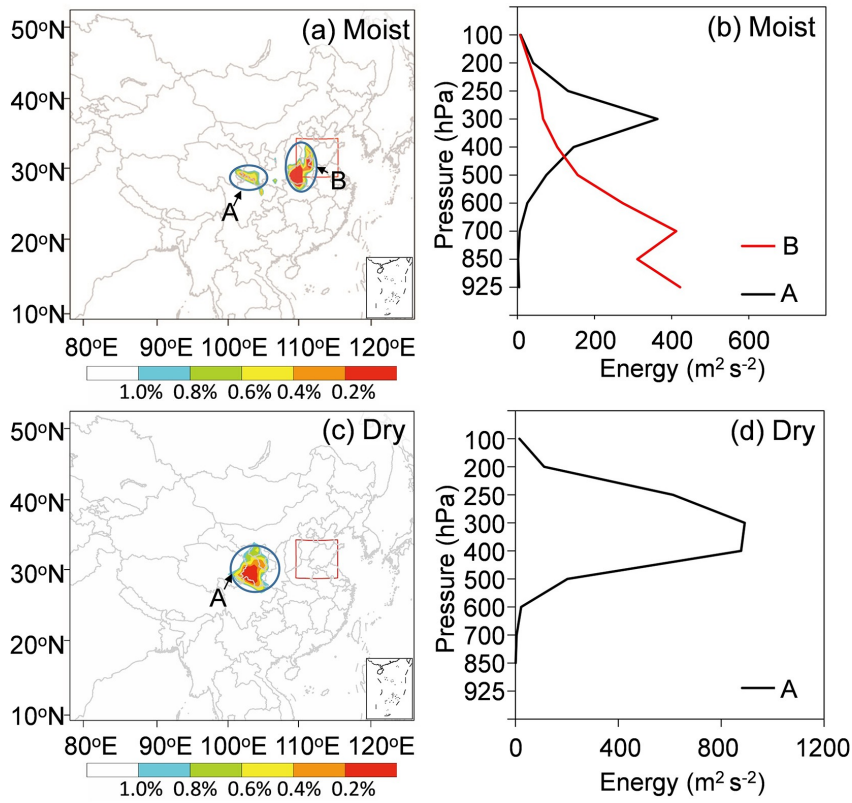


Fig. 3. Sensitive areas (shaded, the top 1% $vTDE'$) identified by the CNOP in (a) EXP_moist and (c) EXP_dry for the “7.06” case. The inner red square box in (a) and (c) denotes the verification area. The blue circles in (a) and (c) denote the sensitive areas. The vertical distribution of $hTDE'$ (units: $m^2 s^{-2}$) over sensitive area A (black line) and B (red line) in panel (a) is shown in (b). (d) is as (b) but for sensitive area A in panel (c).

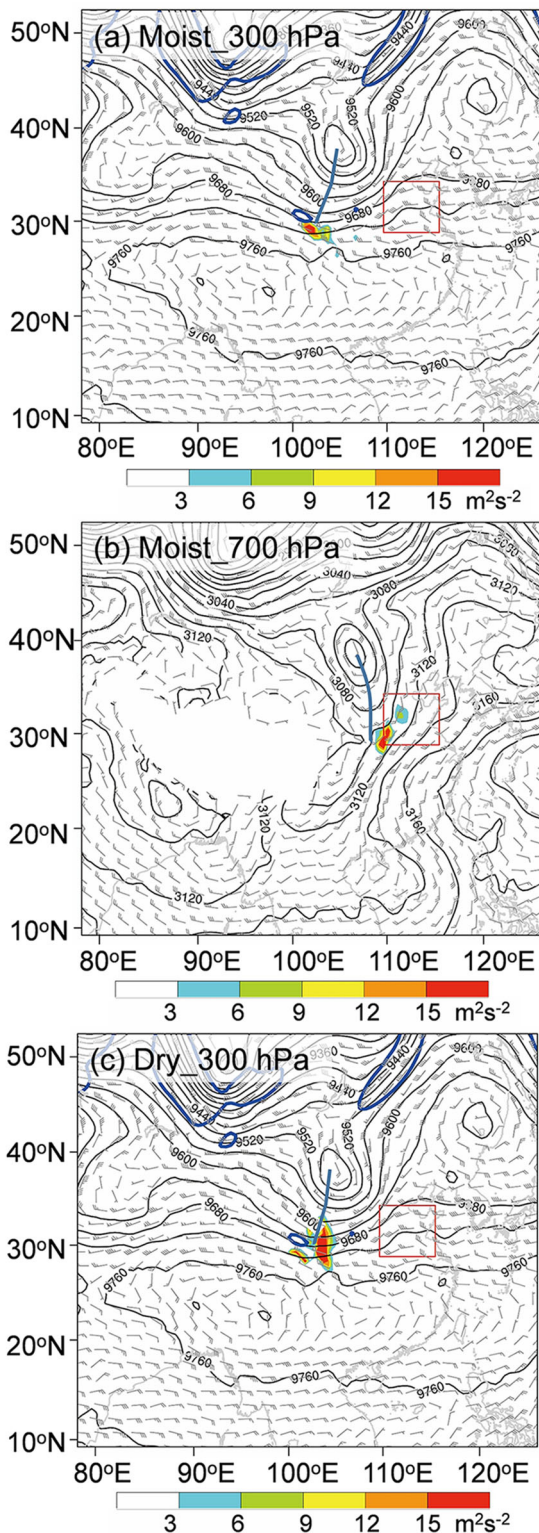


Fig. 4. Wind (barb, a half barb denotes 2 m s⁻¹, a full barb denotes 4 m s⁻¹, and a flag denotes 20 m s⁻¹), geopotential height (contour; units: gpm), and TDE' (shaded; units: m² s⁻²) of the CNOP for the “7.06” case in EXP_moist at (a) 300 hPa and (b) 700 hPa, and in EXP_dry at (c) 300 hPa. The blue contours in (a) and (c) denote wind speed of 30 m s⁻¹. The blue line in (a), (b), and (c) denotes the westerly trough extending from the subtropical cyclone. The inner red box denotes the verification area.

tures the sensitive area in front of the trough extending from the subtropical cyclone at lower levels.

The results of the other three cases are consistent with those of the “7.06” case. The CNOP with moist physics captures the sensitive areas corresponding to both the upper-level and the lower-level weather systems (Figs. 5a–c; Fig. 6a; Fig. 7a; Fig. 8a), while the CNOP without moist physics only captures the sensitive area corresponding to the upper-level weather systems (Figs. 5d–f; Fig. 6b; Fig. 7b; Fig. 8b). The CNOPs with and without moist physics all capture the sensitive areas corresponding to the upper-level systems, such as the westerly trough in the “7.06” (Figs. 4a and 4c) and “7.21” cases (Figs. 8c and 8f), the westerly trough and tropical cyclone (by the CNOP with moist physics, Fig. 6c) and the easterly wind (by the CNOP without moist physics, Fig. 6e) in the “8.14” case, and the jet stream in the “7.09” case (Figs. 7c and 7e). The CNOPs with and without moist physics also capture the sensitive area corresponding to the midlevel trough in the “7.21” case (Figs. 8d and 8g). However, only the CNOPs with moist physics capture the lower-level key weather systems such as the westerly trough in the “7.06” case (Fig. 4b), the tropical cyclone and its inverted trough in the “8.14” case (Fig. 6d), the shear line in the “7.09” case (Fig. 7d), and the lower-level vortex in the “7.21” case (Fig. 8e).

4.2. The importance of moist processes in identifying sensitive areas

As we know, lower-level processes are quite important in the forecast accuracy of heavy rainfall (Liu et al., 2003; Zhang et al., 2016a; Sun et al., 2019), but the CNOP without moist physics fails to capture the lower-level weather systems. For example, in the “7.21” case, the CNOP with moist physics identifies the sensitive areas associated with the upper-level jet stream, midlevel trough, and lower-level vortex, while the CNOP without moist physics only captures the sensitive areas associated the upper-level and midlevel synoptic weather systems (Fig. 8). The primary difference between the CNOPs with and without moist physics is in their identification of the sensitive area associated with the lower-level vortex. According to Yu and Meng (2016), the identified key weather systems in EXP_moist are consistent with those identified by the linear correlation analysis. This also shows that among these weather systems, the lower-level vortex is the most important weather system that influences the forecasting of heavy rainfall. Consequently, EXP_dry misses the most important key factor. In order to understand why the lower-level sensitive area is missed in EXP_dry, the algorithm and physics aspects are examined.

In the algorithm aspect, the gradient of the cost function with respect to initial perturbations is different between the experiments with and without moist physics for the “7.06” case (Fig. 9). In EXP_dry, the gradient peaks at the upper levels, which suggests that the error growth is faster at the upper levels and results in the upper-level peak of the CNOP. In EXP_moist, the gradient peaks at both the upper

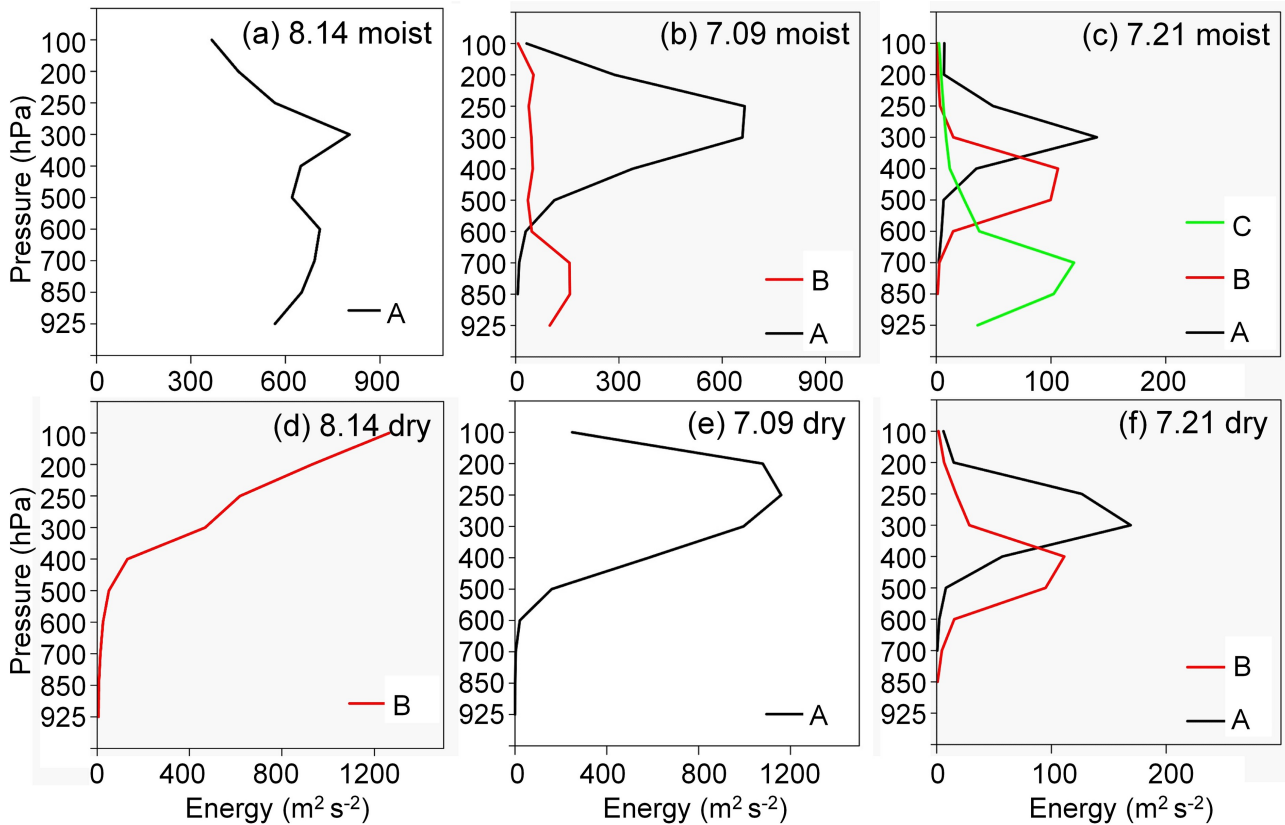


Fig. 5. Vertical distribution of $hTDE'$ (units: $m^2 s^{-2}$) over the corresponding sensitive area in (a–c) EXP_moist and (d–f) EXP_dry for (a, d) the “8.14” case, (b, e) the “7.09” case, and (c, f) the “7.21” case. The black/red/green line represents the vertical distribution of $hTDE'$ (units: $m^2 s^{-2}$) over sensitive area A/B/C in the corresponding experiment.

and lower levels, resulting in both the upper- and lower-level peaks of the CNOP. The results of the other three cases (figure omitted) are consistent with the “7.06” case. For the “7.21” case, the gradients also peak at the midlevels in both experiments, which results in the midlevel peaks of the CNOPs.

In the physics aspect, the distribution of the sensitive area for the “7.06” case at upper levels is generally consistent with the baroclinicity index (Hoskins and Valdes, 1990; Hoskins et al., 2000) shown in Fig. 10a. This is consistent with previous results, which show that for the dry dynamics, the SV structures are typically located upstream and in regions of high baroclinicity (Hoskins et al., 2000; Coutinho et al., 2004). The baroclinicity index is much smaller at lower levels (Fig. 10b), and the lower-level sensitive area is located in regions of large specific humidity (Fig. 10c). Results for the other three cases (figure omitted) are generally consistent with those of the “7.06” case in that the upper-level sensitive area is located upstream and in regions of high baroclinicity and the lower-level sensitive area is located in regions of large specific humidity. These results suggest that the upper-level sensitive area is associated with high baroclinicity, large variable gradients near the tropopause such as large temperature gradient, and large wind shear associated with jets, which cannot be resolved well by

numerical models and thus cause large error growth. These dynamic features can be captured by both CNOPs with and without moist physics. The lower-level sensitive area is associated with moist processes, which is usually accompanied with large error growth. This thermodynamic feature can be captured only by the CNOP with moist physics.

5. Summary

This study examined the influence of moist physical processes on the sensitive area identified by the CNOP method based on four typical heavy rainfall cases in northern China. Results show that the CNOP with moist physics identified sensitive areas corresponding to both lower-level (850–700 hPa) and upper-level (300–100 hPa) weather systems such as an upper-level westerly trough or jet stream, while the CNOP without moist physics only captured the upper-level weather systems and failed to capture the sensitive areas at lower levels that are associated with weather systems such as a westerly trough, tropical cyclone and its inverted trough, shear line, or lower-level vortex.

The reasons for the difference in identifying sensitive areas with and without moist physics can be explained in both algorithm and physics aspects. In the algorithm aspect, the gradients of the cost function with respect to initial per-

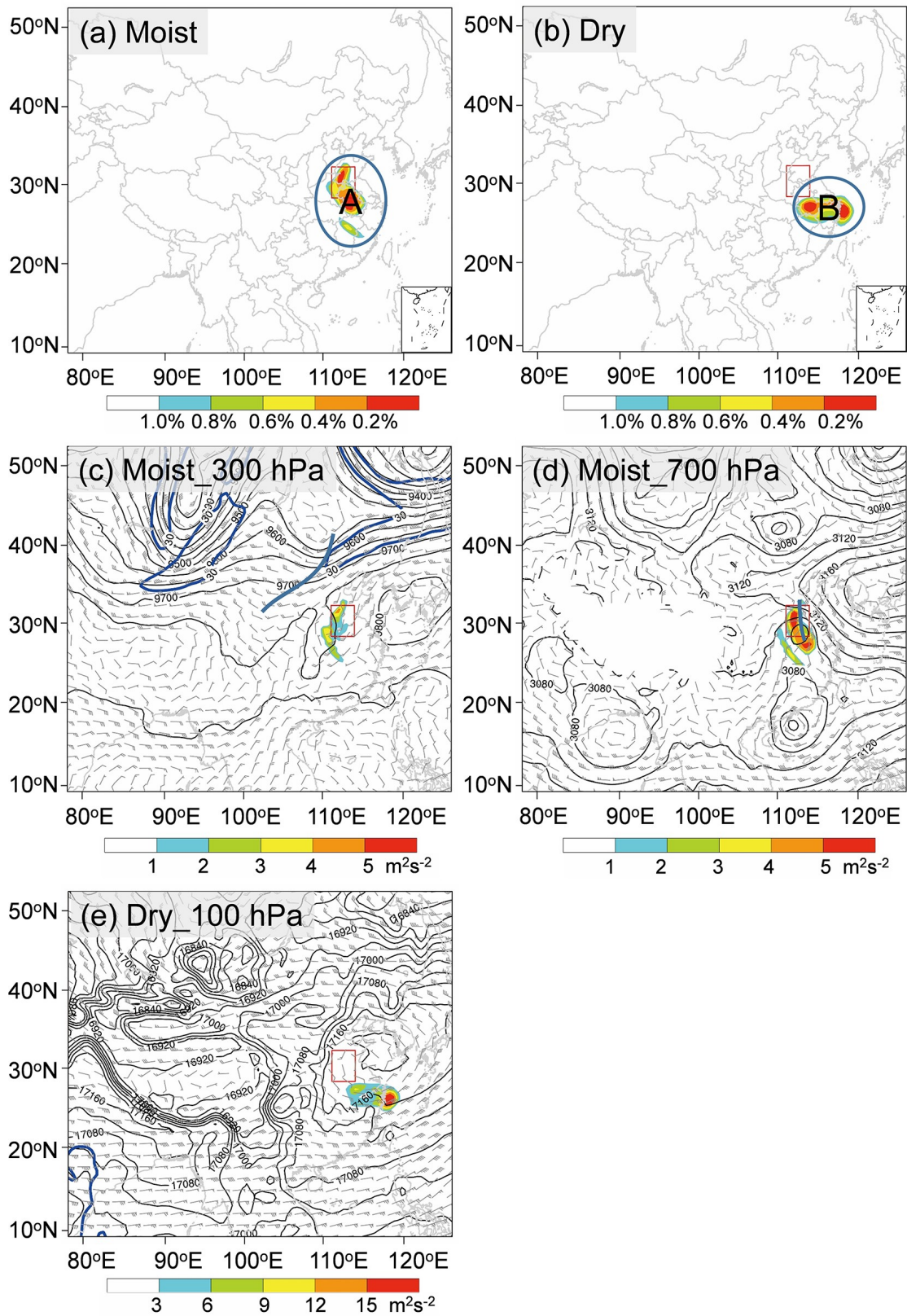


Fig. 6. Sensitive areas (shaded) identified by the CNOP in (a) EXP_moist and (b) EXP_dry for the “8.14” case. Also shown are wind (barb, a half barb denotes 2 m s^{-1} , a full barb denotes 4 m s^{-1} , and a flag denotes 20 m s^{-1}), geopotential height (contour; units: gpm), and TDE' (shaded; units: $\text{m}^2 \text{ s}^{-2}$) of the CNOP in EXP_moist at (c) 300 hPa, (d) 700 hPa, and (e) in EXP_dry at 100 hPa. The inner red box denotes the verification area. The blue circles in (a) and (b) denote the sensitive areas. The blue contours in (c) and (e) denote wind speed of 30 m s^{-1} . The blue line in (c) denotes the westerly trough. The blue line in (d) denotes the inverted trough of the tropical cyclone.

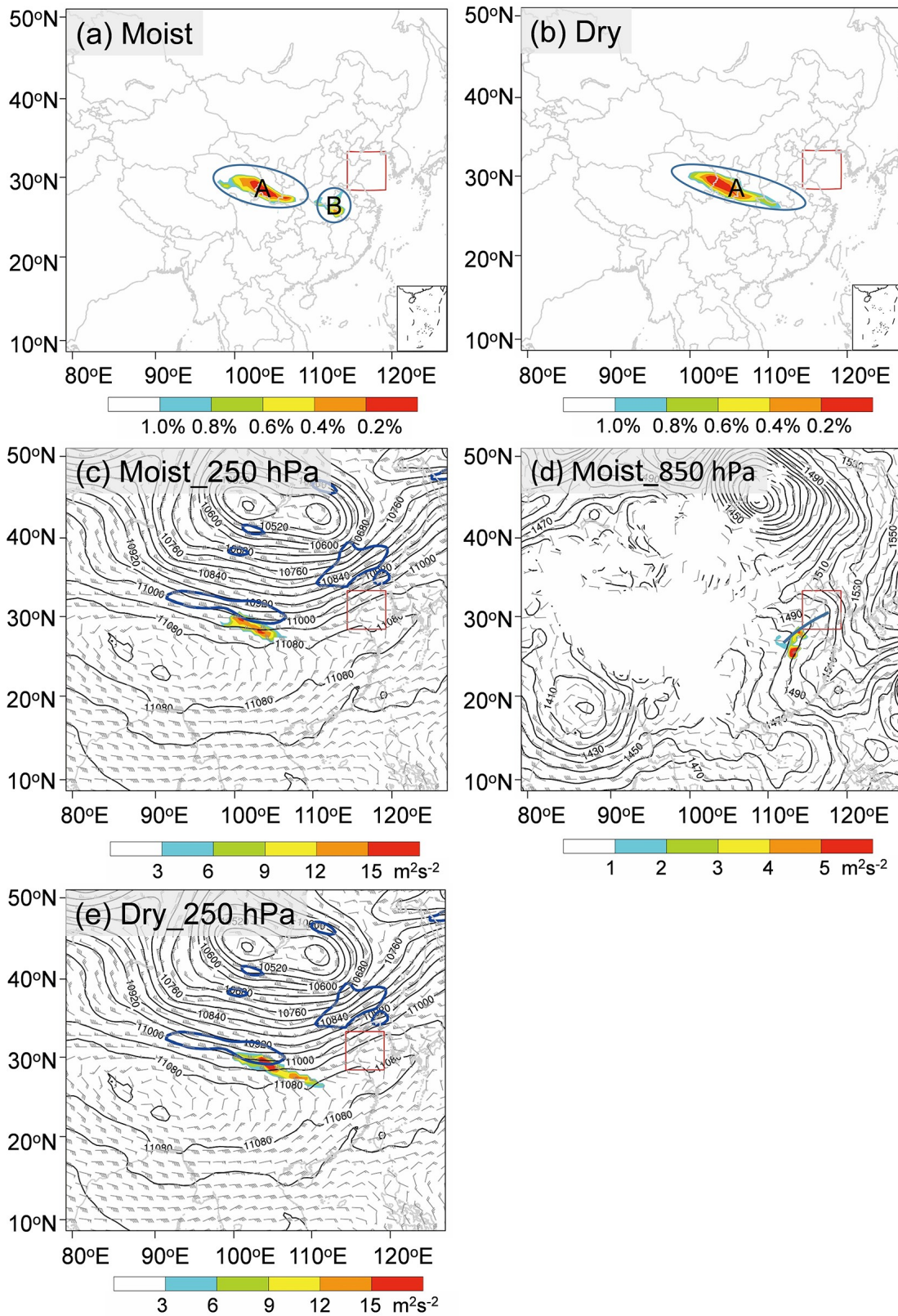


Fig. 7. Sensitive areas (shaded) identified by the CNOP in (a) EXP_moist and (b) EXP_dry for the “7.09” case. Also shown are wind (barb, a half barb denotes 2 m s^{-1} , a full barb denotes 4 m s^{-1} , and a flag denotes 20 m s^{-1}), geopotential height (contour; units: gpm), and TDE' (shaded; units: $\text{m}^2 \text{ s}^{-2}$) of the CNOP in EXP_moist at (c) 250 hPa and (d) 850 hPa, and in EXP_dry at (e) 250 hPa. The blue contours in (c) and (e) denote wind speed of 35 m s^{-1} . The blue line in (d) denotes the shear line. The inner red box denotes the verification area. The blue circles in (a) and (b) denote the sensitive areas.

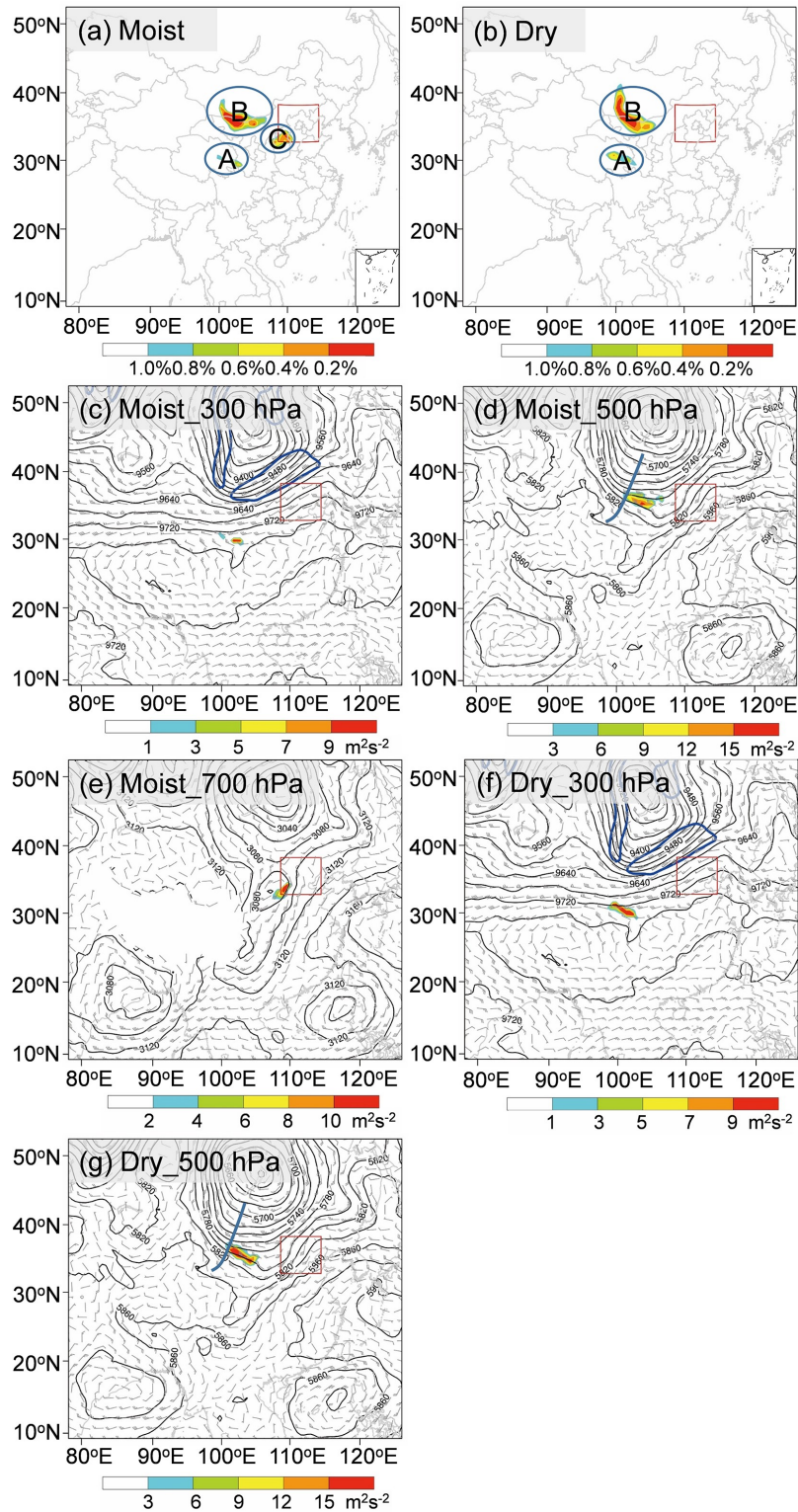


Fig. 8. Sensitive areas (shaded) identified by the CNOP in (a) EXP_moist and (b) EXP_dry for the “7.21” case. Also shown are wind (barb, a half barb denotes 2 m s^{-1} , a full barb denotes 4 m s^{-1} , and a flag denotes 20 m s^{-1}), geopotential height (contour; units: gpm), and TDE' (shaded; units: $\text{m}^2 \text{ s}^{-2}$) of the CNOP in EXP_moist at (c) 300 hPa, (d) 500 hPa, and (e) 700 hPa, and in EXP_dry at (f) 300 hPa and (g) 500 hPa. The blue contours in (c) and (f) denote wind speed of 30 m s^{-1} . The blue line in (d) and (g) denotes the trough extending from the cold vortex. The inner red box denotes the verification area. The blue circles in (a) and (b) denote the sensitive areas.

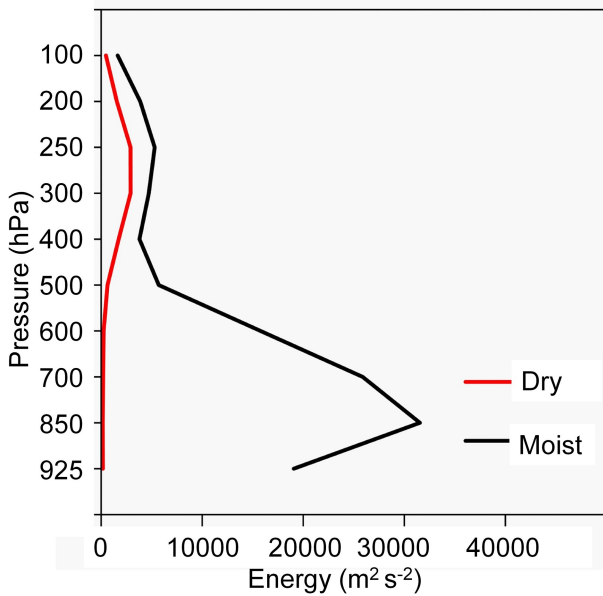


Fig. 9. Vertical distributions of the horizontally integrated gradient of cost function with respect to initial perturbations (units: $\text{m}^2 \text{s}^{-2}$) in EXP_moist (black line) and EXP_dry (red line) for the “7.06” case.

turbations are different with and without moist physics. The gradient peaks at both the upper and lower levels with moist physics, while it only peaks at upper levels without moist physics. In the physics aspect, the upper-level sensitive area is associated with high baroclinicity, and these dynamic features can be captured by both the CNOPs with and without moist physics. The lower-level sensitive area is associated with moist processes, and this thermodynamic feature can be captured only by the CNOP with moist physics. This result demonstrates the important contribution of the initial error of lower-level systems that are related to water vapor transportation to the forecast error of heavy rainfall associated weather systems, which could be an important reference for heavy rainfall observation targeting.

Acknowledgements. This paper is dedicated to Dr. Fuqing ZHANG. Dr. Fuqing ZHANG made tremendous contributions to atmospheric dynamics, predictability, and ensemble-based data assimilation. He developed a widely accepted conceptual model of multiscale multistage error growth in which moist processes impact atmospheric predictability at increasingly larger scales, and for the first time demonstrated that upscale growth of small-scale, small-amplitude initial condition errors through moist convection may fundamentally limit the predictability of severe weather at meso-scale and beyond. This work was supported by the National Natural Science Foundation of China (Grant Nos. 42030604, 41875051, and 41425018). The global analysis data used in this study are the National Centers for Environmental Prediction Final Operational Global Analysis (NCEP FNL), available at <https://rda.ucar.edu/datasets/ds083.2/>. Precipitation data were provided by the National Meteorological Information Center of China Meteorological Administration (<http://data.cma.cn/en/?r=data/detail&dataCode=A.0012.0001>).

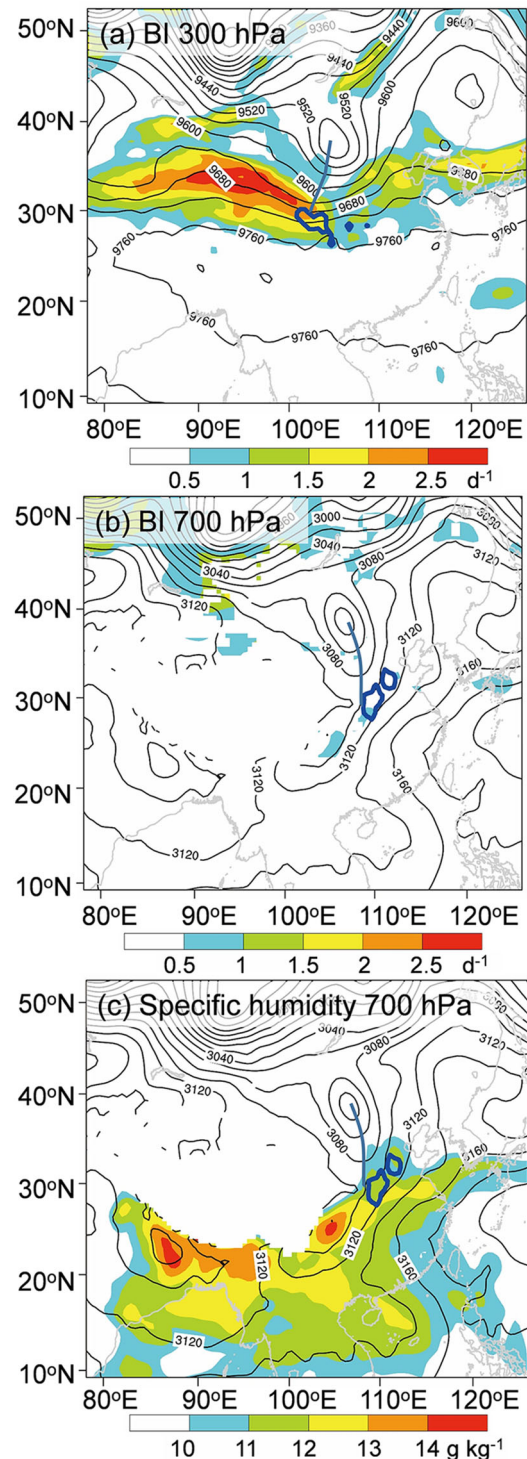


Fig. 10. For the “7.06” case. The baroclinicity index $BI \equiv 0.31f(\partial u/\partial z)N^{-1}$ (f is the Coriolis parameter, N is the Brunt-Vaisala frequency, and $\partial u/\partial z$ is the vertical shear of the wind u) (shaded; units: d^{-1}) and geopotential height (contour; units: gpm) at initial time at (a) 300 hPa and (b) 700 hPa. (c) The geopotential height (contour; units: gpm) at 700 hPa and specific humidity below 700 hPa (shaded; units: g kg^{-1}) at the initial time. The blue contours denote TDE' of the CNOP in EXP_moist of $3 \text{ m}^2 \text{ s}^{-2}$ at (a) 300 hPa, (b) 700 hPa, and (c) 700 hPa. The blue line in (a), (b), and (c) denotes the westerly trough extending from the subtropical cyclone.

REFERENCES

- Birgin, E. G., J. E. Martínez, and M. Raydan, 2001: Algorithm 813: SPG—software for convex-constrained optimization. *ACM Transactions on Mathematical Software*, **27**, 340–349, <https://doi.org/10.1145/502800.502803>.
- Bishop, C. H., B. J. Etherton, and S. J. Majumdar, 2001: Adaptive sampling with the ensemble transform Kalman filter. Part I: Theoretical aspects. *Mon. Wea. Rev.*, **129**, 420–436, [https://doi.org/10.1175/1520-0493\(2001\)129<0420:ASW-TET>2.0.CO;2](https://doi.org/10.1175/1520-0493(2001)129<0420:ASW-TET>2.0.CO;2).
- Buizza, R., and A. Montani, 1999: Targeting observations using singular vectors. *J. Atmos. Sci.*, **56**, 2965–2985, [https://doi.org/10.1175/1520-0469\(1999\)056<2965:TOUSV>2.0.CO;2](https://doi.org/10.1175/1520-0469(1999)056<2965:TOUSV>2.0.CO;2).
- Buizza, R., C. Cardinali, G. Kelly, and J.-N. Thépaut, 2007: The value of observations. II: The value of observations located in singular-vector-based target areas. *Quart. J. Roy. Meteor. Soc.*, **133**, 1817–1832, <https://doi.org/10.1002/qj.149>.
- Cardinali, C., R. Buizza, G. Kelly, M. Shapiro, and J.-N. Thépaut, 2007: The value of observations. III: Influence of weather regimes on targeting. *Quart. J. Roy. Meteor. Soc.*, **133**, 1833–1842, <https://doi.org/10.1002/qj.148>.
- Chen, B.-Y., 2011: Observation system experiments for typhoon nida (2004) using the CNOP method and DOTSTAR data. *Atmos. Ocean. Sci. Lett.*, **4**, 118–123, <https://doi.org/10.1080/16742834.2011.11446914>.
- Chen, Y. F., and G. Gao, 2010: An analysis to losses caused by meteorological disasters in China during 1989–2008. *Meteorological Monthly*, **36**, 76–80, <https://doi.org/10.7519/j.issn.1000-0526.2010.2.011>. (in Chinese with English abstract)
- Coutinho, M. M., B. J. Hoskins, and R. Buizza, 2004: The influence of physical processes on extratropical singular vectors. *J. Atmos. Sci.*, **61**, 195–209, [https://doi.org/10.1175/1520-0469\(2004\)061<0195:TIOppo>2.0.CO;2](https://doi.org/10.1175/1520-0469(2004)061<0195:TIOppo>2.0.CO;2).
- Doyle, J. D., C. A. Reynolds, and C. Amerault, 2019: Adjoint sensitivity analysis of high-impact extratropical cyclones. *Mon. Wea. Rev.*, **147**, 4511–4532, <https://doi.org/10.1175/MWR-D-19-0055.1>.
- Ehrendorfer, M., and R. M. Errico, 1995: Mesoscale predictability and the spectrum of optimal perturbations. *J. Atmos. Sci.*, **52**, 3475–3500, [https://doi.org/10.1175/1520-0469\(1995\)052<3475:MPATSO>2.0.CO;2](https://doi.org/10.1175/1520-0469(1995)052<3475:MPATSO>2.0.CO;2).
- Ehrendorfer, M., R. M. Errico, and K. D. Raeder, 1999: Singular-Vector perturbation growth in a primitive equation model with moist physics. *J. Atmos. Sci.*, **56**, 1627–1648, [https://doi.org/10.1175/1520-0469\(1999\)056<1627:SVPGIA>2.0.CO;2](https://doi.org/10.1175/1520-0469(1999)056<1627:SVPGIA>2.0.CO;2).
- Grell, G. A., J. Dudhia, and D. R. Stauffer, 1995: A description of the fifth-generation Penn State/NCAR Mesoscale Model (MM5). NCAR Tech. Note NCAR/TN-398+STR, 121 pp.
- Hakim, G. J., and R. D. Torn, 2008: Ensemble synoptic analysis. *Meteor. Monogr.*, **33**, 147–162, <https://doi.org/10.1175/0065-9401-33.55.147>.
- Hamill, T. M., and C. Snyder, 2002: Using improved background-error covariances from an ensemble Kalman filter for adaptive observations. *Mon. Wea. Rev.*, **130**, 1552–1572, [https://doi.org/10.1175/1520-0493\(2002\)130<1552:UIBEFC>2.0.CO;2](https://doi.org/10.1175/1520-0493(2002)130<1552:UIBEFC>2.0.CO;2).
- Hoskins, B. J., and P. J. Valdes, 1990: On the existence of stormtracks. *J. Atmos. Sci.*, **47**, 1854–1864, [https://doi.org/10.1175/1520-0469\(1990\)047<1854:OTEOST>2.0.CO;2](https://doi.org/10.1175/1520-0469(1990)047<1854:OTEOST>2.0.CO;2).
- Hoskins, B. J., R. Buizza, and J. Badger, 2000: The nature of singular vector growth and structure. *Quart. J. Roy. Meteor. Soc.*, **126**, 1565–1580, <https://doi.org/10.1002/qj.49712656601>.
- Huang, L., and Z. Y. Meng, 2014: Quality of the target area for metrics with different nonlinearities in a mesoscale convective system. *Mon. Wea. Rev.*, **142**, 2379–2397, <https://doi.org/10.1175/MWR-D-13-00244.1>.
- Joseph, S., and Coauthors, 2015: North Indian heavy rainfall event during June 2013: Diagnostics and extended range prediction. *Climate Dyn.*, **44**, 2049–2065, <https://doi.org/10.1007/s00382-014-2291-5>.
- Jung, B.-J., and H. M. Kim, 2009: Moist adjoint-based forecast sensitivities for a heavy snowfall event over the Korean Peninsula on 4–5 March 2004. *J. Geophys. Res.*, **114**, D15104, <https://doi.org/10.1029/2008JD011370>.
- Kim, H. M., S.-M. Kim, and B.-J. Jung, 2011: Real-Time adaptive observation guidance using singular vectors for typhoon Jangmi (200815) in T-PARC 2008. *Wea. Forecasting*, **26**, 634–649, <https://doi.org/10.1175/WAF-D-10-05013.1>.
- Li, X. S., Y. L. Luo, and Z. Y. Guan, 2014: The persistent heavy rainfall over southern China in June 2010: Evolution of synoptic systems and the effects of the Tibetan Plateau heating. *Journal of Meteorological Research*, **28**, 540–560, <https://doi.org/10.1007/s13351-014-3284-3>.
- Li, X. Z., W. Zhou, Y. Q. Chen, and D. Chen, 2016: Detecting the origins of moisture over southeast China: Seasonal variation and heavy rainfall. *Adv. Atmos. Sci.*, **33**, 319–329, <https://doi.org/10.1007/s00376-015-4197-5>.
- Liu, J. Y., and Z.-M. Tan, 2009: Mesoscale predictability of meiyu heavy rainfall. *Adv. Atmos. Sci.*, **26**, 438–450, <https://doi.org/10.1007/s00376-009-0438-9>.
- Liu, J. Y., Z. M. Tan, and S. N. Gu, 2011: Flow-dependent mesoscale predictability of Meiyu heavy rainfall. *Chinese Journal of Atmospheric Sciences*, **35**, 912–926, <https://doi.org/10.3878/j.issn.1006-9895.2011.05.11>. (in Chinese with English abstract)
- Liu, S.-Y., Y.-G. Zheng, and Z.-Y. Tao, 2003: The analysis of the relationship between pulse of LLJ and heavy rain using wind profiler data. *Journal of Tropical Meteorology*, **9**, 158–163, <https://doi.org/10.3969/j.issn.1006-8775.2003.02.006>.
- Lorenz, E. N., 1963: Deterministic nonperiodic flow. *J. Atmos. Sci.*, **20**, 130–141, [https://doi.org/10.1175/1520-0469\(1963\)020<0130:DNF>2.0.CO;2](https://doi.org/10.1175/1520-0469(1963)020<0130:DNF>2.0.CO;2).
- Lynch, S. L., and R. S. Schumacher, 2014: Ensemble-based analysis of the May 2010 extreme rainfall in Tennessee and Kentucky. *Mon. Wea. Rev.*, **142**, 222–239, <https://doi.org/10.1175/MWR-D-13-00020.1>.
- Mahfouf, J.-F., and B. Bilodeau, 2007: Adjoint sensitivity of surface precipitation to initial conditions. *Mon. Wea. Rev.*, **135**, 2879–2896, <https://doi.org/10.1175/MWR3439.1>.
- Meng, X. F., Y. G. Sun, Sarina, H. M. Yuan, and Hasi, 2013: Correlation between eastward developing of Hetao cyclone and the severe rainstorm in Beijing on 21 July 2012. *Meteorological Monthly*, **39**, 1542–1549, <https://doi.org/10.7519/j.issn.1000-0526.2013.12.002>. (in Chinese with English abstract)
- Molteni, F., R. Buizza, T. N. Palmer, and T. Petroliaigis, 1996: The ECMWF ensemble prediction system: Methodology and validation. *Quart. J. Roy. Meteor. Soc.*, **122**, 73–119, <https://doi.org/10.1002/qj.49712252905>.
- Montani, A., A. J. Thorpe, R. Buizza, and P. Undén, 1999: Forecast skill of the ECMWF model using targeted observations during FASTEX. *Quat. J. Roy. Meteor. Soc.*, **125**,

- 3219–3240, <https://doi.org/10.1002/qj.49712556106>.
- Mu, M., and W. S. Duan, 2003: A new approach to studying ENSO predictability: Conditional nonlinear optimal perturbation. *Chinese Science Bulletin*, **48**, 1045–1047, <https://doi.org/10.1007/BF03184224>.
- Mu, M., H.-L. Wang, and F.-F. Zhou, 2007: A preliminary application of conditional nonlinear optimal perturbation to adaptive observation. *Chinese Journal of Atmospheric Sciences*, **31**, 1102–1112, <https://doi.org/10.3878/j.issn.1006-9895.2007.06.06>. (in Chinese with English abstract)
- Ni, Y. Q., X. J. Zhou, R. H. Zhang, P. Y. Wang, and Q. J. Yi, 2006: Experiments and studies for heavy rainfall in southern China. *Journal of Applied Meteorological Science*, **17**, 690–704, <https://doi.org/10.3969/j.issn.1001-7313.2006.06.007>. (in Chinese with English abstract)
- Palmer, T. N., R. Gelaro, J. Barkmeijer, and R. Buizza, 1998: Singular vectors, metrics, and adaptive observations. *J. Atmos. Sci.*, **55**, 633–653, [https://doi.org/10.1175/1520-0469\(1998\)055<0633:SVMAAO>2.0.CO;2](https://doi.org/10.1175/1520-0469(1998)055<0633:SVMAAO>2.0.CO;2).
- Qi, L. B., and J. Xu, 2018: Rethink on short range forecast of the 9 July severe rainstorm in northern Henan. *Meteorological Monthly*, **44**, 1–14, <https://doi.org/10.7519/j.issn.1000-0526.2018.01.001>. (in Chinese with English abstract)
- Reynolds, C. A., and T. E. Rosmond, 2003: Nonlinear growth of singular-vector-based perturbations. *Quart. J. Roy. Meteor. Soc.*, **129**, 3059–3078, <https://doi.org/10.1256/qj.02.193>.
- Reynolds, C. A., J. D. Doyle, F. M. Ralph, and R. Demirdjian, 2019: Adjoint sensitivity of North Pacific atmospheric river forecasts. *Mon. Wea. Rev.*, **147**, 1871–1897, <https://doi.org/10.1175/MWR-D-18-0347.1>.
- Schumacher, R. S., 2011: Ensemble-based analysis of factors leading to the development of a multiday warm-season heavy rain event. *Mon. Wea. Rev.*, **139**, 3016–3035, <https://doi.org/10.1175/MWR-D-10-05022.1>.
- Sippel, J. A., and F. Q. Zhang, 2010: Factors affecting the predictability of hurricane Humberto (2007). *J. Atmos. Sci.*, **67**, 1759–1778, <https://doi.org/10.1175/2010JAS3172.1>.
- Sun, J. H., Y. C. Zhang, R. X. Liu, S. M. Fu, and F. Y. Tian, 2019: A review of research on warm-sector heavy rainfall in China. *Adv. Atmos. Sci.*, **36**, 1299–1307, <https://doi.org/10.1007/s00376-019-9021-1>.
- Wang, C.-C., J. C.-S. Hsu, G. T.-J. Chen, and D.-I. Lee, 2014a: A study of two propagating heavy-rainfall episodes near Taiwan during SoWMEX/TiMREX IOP-8 in June 2008. Part II: Sensitivity tests on the roles of synoptic conditions and topographic effects. *Mon. Wea. Rev.*, **142**, 2644–2664, <https://doi.org/10.1175/MWR-D-13-00330.1>.
- Wang, J. Y., C. G. Cui, X. F. Wang, and W. J. Cui, 2014b: Analysis on water vapor transport and budget of the severe torrential rain over Beijing region on 21 July 2012. *Meteorological Monthly*, **40**, 133–145, <https://doi.org/10.7519/j.issn.1000-0526.2014.02.001>. (in Chinese with English abstract)
- Wang, Q., and M. Mu, 2017: Application of conditional nonlinear optimal perturbation to target observations for high-impact ocean-atmospheric environmental events. *Data Assimilation for Atmospheric, Oceanic and Hydrologic Applications (Vol. III)*, S. K. Park and L. Xu, Eds., Springer International Publishing, 513–526, https://doi.org/10.1007/978-3-319-43415-5_23.
- Xu, J., Y. Chen, J. Sun, S. Yang, Z. Zong, T. Chen, C. Fang, and J. Sheng, 2012: Observation analysis of Beijing extreme flooding event 21 July 2012. *Weather Forecast Review*, **4**, 9–19. (in Chinese)
- Yu, H. Z., and Z. Y. Meng, 2016: Key synoptic-scale features influencing the high-impact heavy rainfall in Beijing, China, on 21 July 2012. *Tellus A: Dynamic Meteorology and Oceanography*, **68**, 31045, <https://doi.org/10.3402/tellusa.v68.31045>.
- Yu, H. Z., H. L. Wang, Z. Y. Meng, M. Mu, X.-Y. Huang, and X. Zhang, 2017: A WRF-based tool for forecast sensitivity to the initial perturbation: The conditional nonlinear optimal perturbations versus the first singular vector method and comparison to MM5. *J. Atmos. Oceanic Technol.*, **34**, 187–206, <https://doi.org/10.1175/JTECH-D-15-0183.1>.
- Zhang, F., C. Snyder, and R. Rotunno, 2002: Mesoscale predictability of the "surprise" snowstorm of 24–25 January 2000. *Mon. Wea. Rev.*, **130**, 1617–1632, [https://doi.org/10.1175/1520-0493\(2002\)130<1617:MPOTSS>2.0.CO;2](https://doi.org/10.1175/1520-0493(2002)130<1617:MPOTSS>2.0.CO;2).
- Zhang, F., C. Snyder, and R. Rotunno, 2003: Effects of moist convection on mesoscale predictability. *J. Atmos. Sci.*, **60**, 1173–1185, [https://doi.org/10.1175/1520-0469\(2003\)060<1173:EOMCOM>2.0.CO;2](https://doi.org/10.1175/1520-0469(2003)060<1173:EOMCOM>2.0.CO;2).
- Zhang, F. Q., A. M. Odins, and J. W. Nielsen-Gammon, 2006: Mesoscale predictability of an extreme warm-season precipitation event. *Wea. Forecasting*, **21**, 149–166, <https://doi.org/10.1175/WAF909.1>.
- Zhang, G. C., 2006: Prevention and mitigation of the meteorological disasters—The world meteorological day, 2006. *Meteorological Monthly*, **32**, 3–5, <https://doi.org/10.7519/j.issn.1000-0526.2006.03.001>. (in Chinese with English abstract)
- Zhang, M. R., and Z. Y. Meng, 2018: Impact of synoptic-scale factors on rainfall forecast in different stages of a persistent heavy rainfall event in South China. *J. Geophys. Res.*, **123**, 3574–3593, <https://doi.org/10.1002/2017JD028155>.
- Zhang, X. B., Y. L. Luo, Q. L. Wan, W. Y. Ding, and J. X. Sun, 2016a: Impact of assimilating wind profiling radar observations on convection-permitting quantitative precipitation forecasts during SCMREX. *Wea. Forecasting*, **31**, 1271–1292, <https://doi.org/10.1175/WAF-D-15-0156.1>.
- Zhang, Y. J., F. Q. Zhang, D. J. Stensrud, and Z. Y. Meng, 2016b: Intrinsic predictability of the 20 May 2013 tornadic thunderstorm event in Oklahoma at storm scales. *Mon. Wea. Rev.*, **144**, 1273–1298, <https://doi.org/10.1175/MWR-D-15-0105.1>.
- Zhou, F. F., and H. Zhang, 2014: Study of the schemes based on CNOP method to identify sensitive areas for typhoon targeted observations. *Chinese Journal of Atmospheric Sciences*, **38**, 261–272, <https://doi.org/10.3878/j.issn.1006-9895.2013.13129>. (in Chinese with English abstract)
- Zhu, B. L., W. T. Lin, and Y. Zhang, 2009: Impacts of initial perturbations on prediction of a heavy rain in South China. *Chinese Journal of Atmospheric Sciences*, **33**, 1333–1347, <https://doi.org/10.3878/j.issn.1006-9895.2009.06.18>. (in Chinese with English abstract)
- Zhu, H. F., D. Y. Wang, Z. Y. Guan, Y. Liu, and Y. F. Fu, 2007: Effects of different initial fields on GRAPES numerical prediction. *Journal of Meteorological Research*, **21**, 496–506.
- Zou, X. L., F. Vandenbergh, M. Ponca, and Y.-H. Kuo, 1997: Introduction to adjoint techniques and the MM5 adjoint modeling system. NCAR Tech. Note NCAR/TN2435+STR, 110 pp.